SUBMITTED TO THE ASTROPHYSICAL JOURNAL
Preprint typeset using LaTeX style emulateapj v. 11/10/09

MULTIWAVELENGTH OBSERVATIONS OF THE BLACK HOLE XTE J1752-223 DURING ITS 2010 OUTBURST DECAY, A NEW LOWER LIMIT ON THE DISTANCE

Y. Y. CHUN[1], T. DINÇER[1], E. KALEMCI[1], T. GÜVER[1], J. A. TOMSICK[2], M. M. BUXTON[3], C. BROCKSOPP[4], S. CORBEL[5] AND A. CABRERA-LAVERS[6]

submitted to the Astrophysical Journal

ABSTRACT

Galactic black hole transients show many interesting phenomena during outburst decays. We present simultaneous X-ray (RXTE, Swift, and INTEGRAL), and optical/near-infrared (O/NIR) observations (SMARTS), of the X-ray transient, XTE J1752-223 during its outburst decay in 2010. The multi-wavelength observations of 150 days in 2010 cover the transition from soft to hard spectral state. The evolution of ATCA/VLBI radio observations are shown to confirm the compact jet appearance. The source shows flares in O/NIR during changes in X-ray and radio properties. One of those flares is bright and long, and starts about 20 days after the transition in timing. Other, smaller flares occur along with the transition in timing and increase in power-law flux, and also right after the detection of the core with VLBI. Furthermore, using the simultaneous broadband X-ray spectra including *INTEGRAL*, we found that a high energy cut-off is necessary with a folding energy at around 250 keV around the time that the compact jet is forming. The broad band spectrum can also be fitted equally well with a Comptonization model. In addition, using photoelectric absorption edges in the XMM–Newton RGS X-ray spectra and the extinction of red clump giants in the direction of the source, we found a lower limit on the distance of > 5 kpc.

Subject headings: black hole physics – X-rays:stars – accretion, accretion disks – binaries:close

1. INTRODUCTION

Galactic black hole transients (hereafter GBHTs) show distinct spectral and temporal properties during the whole outburst, across all wavelengths. According to their spectral and timing properties these systems are found mainly in the hard state (HS) or the soft state (SS). In the HS, the X-ray spectrum is dominated by a hard component, which may be caused by Comptonization of soft photons (from the disk or the jet) by a hot electron corona which can also be the base of the jet. If fitted with a power-law, the photon index (Γ) is less than 2.0. The lightcurves also show strong variability (>20% rms amplitude). On the other hand, in the SS, the X-ray spectrum is dominated by soft photons from a geometrically thin, optically thick disk, and the timing variability is very low, mostly below the detection limit of *RXTE* for short observations. In addition, there exists intermediate states (IS), in which sources behave as a combination of these two states. These spectral states are described in more detail in McClintock & Remillard (2006) and Belloni (2010).

During the outburst decays, these sources display state transitions in spectral and temporal properties from the SS to IS to HS. Usually a compact jet is observed in the HS, its signatures can be detected throughout the electromagnetic spectrum, in radio, near infrared (NIR), even maybe in X-rays (Fender 2001; Coriat et al. 2009; Russell et al. 2010). Since the jet emission is quenched in the SS (Russell et al. 2011), multiwavelength investigation of outburst decays allows us to investigate the X-ray spectral and timing properties for jet formation, and its contribution to the X-ray emission.

A possible effect of the jet on the X-ray spectral properties is the injection of non-thermal electrons in the corona, thereby hardening the X-ray spectrum. A cut-off in high energy spectrum of these sources is often observed in the hard state, usually interpreted as a sign of thermal Comptonization. Sometimes the cut-off disappears in high energies after jets are observed (4U 1543−47 Kalemci et al. 2005, GRO 1655−40 Kalemci et al. 2006b; Caballero García et al. 2007). However, there are sources that do not require a cut-off for the entire outburst (H1743−322 Kalemci et al. 2006a, GX 339-4 during its decay in 2005 Kalemci et al. 2006b, XTE J1720−318 Cadolle Bel et al. 2004). Miyakawa et al. (2008) investigated the presence of cut-off from all bright hard state observations of GX 339-4 observed with HEXTE on *RXTE*, yet the statistics were not good enough to constrain the evolution of the cut-off parameters. On the other hand, *INTEGRAL*, and HEXTE on *RXTE* provided interesting results from the hard state to hard intermediate state in the rising phase of the outburst of GX 339-4 (Motta et al. 2009). However, even in the brighter outburst rise, the relation between high energy cut-off parameters and presence of jets is not well established. For example with the same data set, but slightly different set of instruments Caballero García et al. (2007) and Joinet et al. (2008) reached conflicting results about the presence of cut-offs in the hard state spectrum of GRO J1655-40 during the

[1] Sabanci University, Faculty of Engineering and Natural Sciences, Orhanli, Istanbul, 34956, Turkey
[2] Space Sciences Laboratory, 7 Gauss Way, University of California, Berkeley, CA, 94720-7450, USA
[3] Yale University, Yale, USA
[4] Mullard Space Science Laboratory, University College London, Holmbury St Mary, Dorking, Surrey RH5 6NT, UK
[5] AIM - Unité Mixte de Recherche CEA - CNRS - Université Paris VII - UMR 7158, CEA Saclay, Service d'Astrophysique, F-91191 Gif sur Yvette, France
[6] Instituto de Astrofisica de Canarias, E-38205 La Laguna, Tenerife, Spain

outburst rise.

Measuring distances of Galactic black hole sources provides important information about the birthplaces of X-ray binaries, and more importantly allows us to constrain the luminosities of these sources. Obtaining the X-ray luminosity of these sources would allow us to tie spectral states to physical processes in the accretion physics. It was shown by Maccarone (2003) that transition luminosities occur at similar values. This can be related to the changes from an accretion regime dominated by the disk to the one dominated by an ADAF. Furthermore, this could also help in understanding the jet physics, at which luminosities they can form, and if jet dominated states exist at low luminosities (e. g. Russell et al. 2010), at what luminosity this takes place. Moreover luminosities are important to study the fundamental plane that connects the radio - X-ray correlation Corbel et al. (2000, 2003) from stellar mass black holes to the supermassive black holes (Merloni et al. 2003; Falcke et al. 2004; Körding et al. 2006), as well as the variability studies that connects these black hole sources (Körding et al. 2007).

1.1. *XTE J1752-223*

XTE J1752-223 was discovered in the Galactic bulge region by the Rossi X-ray Timing Explorer (RXTE) on 23 October 2009 (Markwardt et al. 2009b). It was suggested to be a black hole candidate by Markwardt et al. (2009a). Strong, relativistic iron emission lines are detected by *Suzaku* and *XMM-Newton* (Reis et al. 2011). The source showed typical outburst evolution of GBHTs, and intensely monitored using several satellites, RXTE (Muñoz-Darias et al. 2010; Shaposhnikov 2010), MAXI (Nakahira et al. 2010) and Swift (Curran et al. 2011). A distance of 3.5±0.4 kpc and mass of the black hole, 8–11$M_{\odot}$, were determined by Shaposhnikov et al. (2010) using QPO frequency saturation and comparison with other sources. Ratti et al. (2012) recently discussed the X-ray – radio correlation in this source. They also suggested that the source is in the Galactic bulge or closer to us, i.e. < 8 kpc, in addition to that the distance estimate by Shaposhnikov et al. (2010) is probably a lower limit. The source's core location was accurately determined using the astrometric optical observations and the VLBI radio imaging (Miller-Jones et al. 2011), in addition to the detection of decelerating, expanding jets and receding ejecta (Yang et al. 2011).

Russell et al. (2012) discussed a late jet re-brightening in the HS via multiwavelength observations during its outburst decay towards quiescence. They suggested that the brightening in the optical and X-rays probably have a common origin, the synchrotron jet, arguing very similar light curve morphology in these two bands, or the corona and the jet might have a close correlation during the flare. They also suggested a changing jet power at the peak of jet flare, proclaiming an evidence of the jet break between optically thin and thick synchrotron emission shifted to higher frequencies.

In this paper, we present an in-depth multiwavelength analysis of XTE J1752-223 during its outburst decay, covered well with *RXTE* and *SWIFT* in X-rays, SMARTS in near infrared (NIR) and optical, and*ATCA* in radio. The spectral and temporal analyses for the source were examined for the whole outburst decay by simultaneous monitoring of RXTE and Swift during MJD55,240–55,390. The behavour is compared to the evolution in NIR and optical, as well as the radio. An additional 3-day (MJD55,305–55,307) broadband X-ray spectrum (*SWIFT*, *RXTE*, and *INTEGRAL*), covering 0.6 – 200 keV, was also investigated in order to find out the high energy behavior of the source. Moreover, we analyzed the *XMM* RGS spectra to determine the Hydrogen column density (N_H) of the source and used this information to determine the distance. We compared the result with the previously reported distance estimates (Shaposhnikov et al. 2010; Ratti et al. 2012)

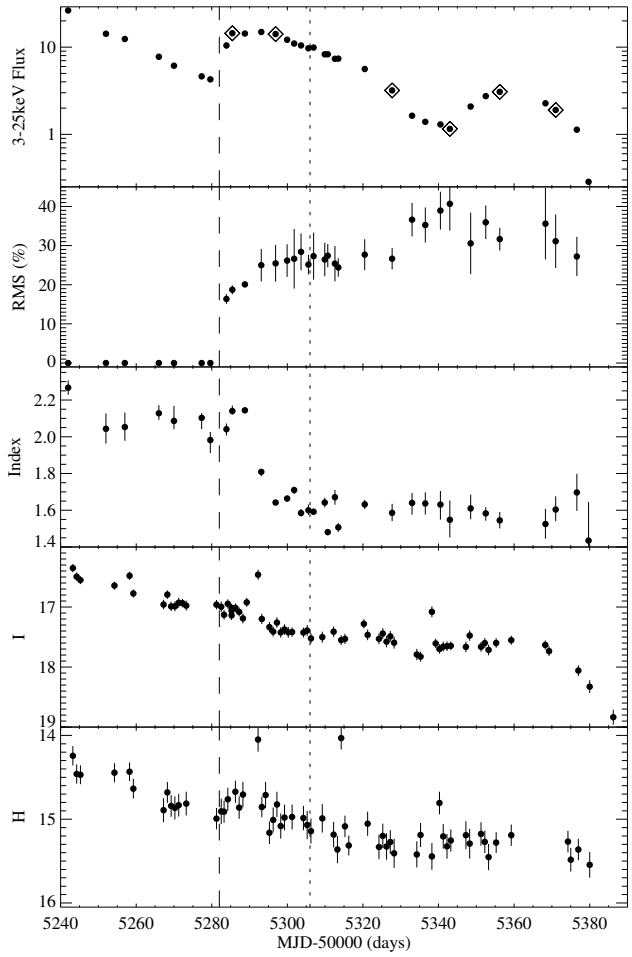

Figure 1. The evolution of spectral and temporal properties of XTE J1752-223. The photon index was obtained from combined X-ray spectra of XRT and PCA. The rms and flux after MJD55,303 were corrected due to the ridge emission in PCA. The fast transition determined by timing analysis is indicated by a dashed line on MJD 55,282. The dotted line shows the time of the *INTEGRAL* observations. The two panels on the bottom are of the I and H band NIR lightcurves, respectively. The observations shown in diamonds in the top panel correspond to those for which we show the power spectra in Fig.3

2. DATA REDUCTION

2.1. *RXTE*

The X-ray evolution of XTE J1752–223 in 2010 outburst is shown in the top three panels of Fig. 1: unabsorbed flux in 3-25 keV, rms amplitude of variability, and power-law index, respectively. The source was monitored

Table 1
Journal of X-ray spectral and temporal parameters

MJD	XTE ObsId	Swift ObsId	Flux[a]	rms (%)	Γ	$T_{in}(keV)$	ν_1 (Hz)[b]	note
55242	95360-01-04-04	31532014	26.328	...	$2.27^{+0.04}_{-0.04}$	$0.57^{+0.01}_{-0.01}$	...	
55252	95360-01-05-02	31532021	14.236	...	$2.04^{+0.08}_{-0.08}$	$0.53^{+0.01}_{-0.01}$	...	
55257	95360-01-06-04	31640001	12.397	...	$2.05^{+0.08}_{-0.08}$	$0.52^{+0.01}_{-0.01}$	...	
55266	95360-01-08-00	31640003	7.7581	...	$2.13^{+0.04}_{-0.04}$	$0.49^{+0.01}_{-0.01}$	...	
55270	95360-01-08-03	31640005	6.1194	...	$2.09^{+0.08}_{-0.05}$	$0.48^{+0.01}_{-0.01}$	...	
55277	95360-01-09-03	31640006	4.6238	...	$2.10^{+0.03}_{-0.06}$	$0.48^{+0.01}_{-0.01}$	...	
55580	95360-01-09-05	31640007	4.2723	...	$1.98^{+0.04}_{-0.07}$	$0.49^{+0.01}_{-0.01}$	...	
55284	95360-01-10-02	31640008	10.445	16.36±1.24	$2.04^{+0.03}_{-0.04}$	$0.45^{+0.01}_{-0.01}$	3.15±0.68	
55285	95360-01-10-04	31640009	14.444	18.72±1.15	$2.14^{+0.03}_{-0.02}$	$0.41^{+0.01}_{-0.01}$	**1.83**±0.58	
55289	95360-01-11-00	31640010	14.334	20.09±0.68	$2.14^{+0.01}_{-0.02}$	$0.42^{+0.01}_{-0.01}$	1.67±0.24	
55293	95360-01-11-04	31640011	14.924	25.00±4.15	$1.81^{+0.01}_{-0.02}$	$0.29^{+0.02}_{-0.01}$	0.55±0.22	
55297	95360-01-12-01	31640012	14.129	25.46±4.68	$1.64^{+0.01}_{-0.01}$	$0.31^{+0.04}_{-0.04}$	**0.35**±0.12	
55300	95360-01-12-03	31688001	12.157	26.17±4.17	$1.66^{+0.01}_{-0.02}$	$0.25^{+0.03}_{-0.02}$	0.36±0.13	
55302	95360-01-12-04	31688003	10.993	26.63±7.61	$1.71^{+0.02}_{-0.02}$	$0.26^{+0.03}_{-0.02}$	0.41±0.10	
55304	95702-01-01-01	31688006	10.462	28.40±4.72	$1.59^{+0.02}_{-0.02}$	$0.29^{+0.03}_{-0.03}$	0.35±0.10	ISGRI
55306	95702-01-01-03	31688008	9.7074	25.15±2.51	$1.60^{+0.03}_{-0.03}$	$0.25^{+0.10}_{-0.05}$	0.41±0.17	ISGRI
55307	95702-01-01-04	31688009	9.8888	27.30±6.00	$1.59^{+0.02}_{-0.02}$	$0.25^{+0.02}_{-0.02}$	0.29±0.11	
55310	95702-01-02-00	31640013	8.2724	26.44±4.30	$1.64^{+0.03}_{-0.03}$	$0.31^{+0.08}_{-0.05}$	0.33±0.13	
55311	95702-01-02-01	31640014	8.2815	27.41±2.99	$1.48^{+0.01}_{-0.02}$	$0.27^{+0.04}_{-0.03}$	0.41±0.13	
55313	95702-01-02-03	31688012	7.3498	25.40±4.51	$1.67^{+0.04}_{-0.04}$	$0.25^{+0.07}_{-0.04}$	0.43±0.26	
55313.5	95702-01-02-04	31688013	7.3846	24.41±2.35	$1.51^{+0.02}_{-0.03}$	$0.33^{+0.16}_{-0.06}$	0.32±0.09	
55320.5	95702-01-03-04	31688014	5.6153	27.69±3.95	$1.63^{+0.03}_{-0.03}$	No disk	0.36±0.12	
55328	95702-01-04-04	31688016	3.1901	26.65±2.74	$1.59^{+0.05}_{-0.05}$	needed	**0.29**±0.11	a single
55333	95702-01-05-03	31688017	1.6355	36.62±4.26	$1.64^{+0.05}_{-0.06}$		0.17±0.06	Lorentzian
55336.5	95702-01-05-06	31688018	1.3928	35.26±4.47	$1.64^{+0.06}_{-0.06}$		0.15±0.05	enough
55340.5	95702-01-06-02	31688019	1.2990	38.94±4.83	$1.63^{+0.07}_{-0.08}$		0.15±0.04	
55343	95702-01-06-03	31688020	1.1554	40.67±6.84	$1.55^{+0.11}_{-0.10}$		**0.22**±0.10	
55348.5	95702-01-07-05	31688021	2.0856	30.56±7.86	$1.61^{+0.08}_{-0.06}$		$\leq$1.41	
55352.5	95702-01-08-00	31688022	2.7439	35.94±4.28	$1.58^{+0.03}_{-0.04}$		0.25±0.05	
55356	95702-01-08-02	31688023	3.0706	31.65±2.90	$1.55^{+0.05}_{-0.04}$		**0.19**±0.07	
55368	95702-01-10-01	31688024	2.2719	35.59±9.11	$1.53^{+0.08}_{-0.08}$		0.20±0.12	
55371	95702-01-10-02	31688025	1.9037	31.11±6.84	$1.60^{+0.07}_{-0.06}$		**0.18**±0.10	
55377	95702-01-11-01	31688026	1.1313	27.21±5.00	$1.70^{+0.10}_{-0.10}$		0.09±0.04	
55380	95702-01-12-00	31688027	0.2859	...	$1.44^{+0.21}_{-0.21}$		4.18±1.74	

[a] The unabsorbed flux values between 3–25 keV are in units of 10^{-10} ergs/cm^2/s.
[b] The timing properties of observations. Those shown in bold are discussed further in text and in Fig. 3. nu_1 stands for the peak frequency of the Lorentzian that peaks at lower frequencies.

throughout the outburst decay, including the fast transition from SS to HS at MJD 55,282 until it went below detection after MJD 55,380.

The RXTE PCA data were reduced with the scripts developed at UC San Diego and University of Tübingen using HEASOFT v6.7. In the energy spectra extraction, the photons from all available PCUs were considered. The background spectra were created from "bright" or "faint" models on the basis of net count rate being greater or less than 70/PCU, respectively. We added 0.5% systematic error to all PCA spectra as suggested by the *RXTE* team.

We used Tübingen Timing Tools in IDL to compute the power density spectra (PDS) of all observations using PCA light curves in 3-25 keV band. The dead time effects were removed according to Zhang et al. (1995) with a dead-time of 10 μs per event, and the PDS is normalized according to Miyamoto & Kitamoto (1989). Broad and narrow Lorentzians (quality factor greater than 2 are denoted as QPOs) are used for fitting (Kalemci et al. 2005; Pottschmidt 2002). The rms amplitudes are calculated by integrating rms-normalized PDS from 0 Hz to infinity. The peak frequencies are calculated as described in Belloni et al. (2002).

2.2. *INTEGRAL*

We observed the source using *INTEGRAL* (the INTernational Gamma-Ray Astrophysics Laboratory), observation ID "07400260001" for dates between MJD 55,304 and 55,306 (Rev. 0917, 0918). The IBIS and SPI data were reduced and analyzed with the help of the ISDC Off-line Scientific Analysis (OSA) software package 9.0, and only the ISGRI spectra were used for further analysis in order to get better statistics at the relevant energy range. The entire dataset was first divided into 3 to check whether the spectrum evolves at high energies. Since there was no significant evolution, we decided to merge 2 revolutions in order to increase statistics, i.e.

the total integration time became 177.4ks. The observation time is indicated by a dotted line in Fig. 1. Note that neither spectral nor temporal properties show significant evolution around the time of the *INTEGRAL* observation.

2.3. *SWIFT*

The *SWIFT* XRT data were processed with the standard procedures (xrtpipeline v0.12.3). In the observations we analyzed, Windowed Timing mode data were availble before MJD 55,367 and Photon Counting mode data were used afterwards. The energy spectra of the source were extracted from the photons within a circle of radius 35" centered at the source position. The background spectra were extracted from photons within regions between 70" and 100" from XTE J1752-223 centroid. The selection of event grades was 0-2, and XRT response matrices swxwt0to2s6_20070901v012.rmf, and swxpc0to12s6_20070901v011.rmf were used for the Windowed Timing and Photon Counting modes respectively. We also generated auxiliary response files with the HEASOFT tool xrtmkarf. In making the ARF files, we used an exposure map produced with the tool xrtexpomap. There was also some pile-up before MJD 55,272 when the count rates were over 100, and for these observations we excluded the peak region of radius 5".

2.4. *XMM–Newton*

XMM–Newton observation of the source was performed on 6 April 2010, MJD 55,292. The total exposure time of the observation was 41.8 ks. Details of this observation and results from the EPIC-pn detector has been discussed in Reis et al. (2011). We here concentrate on the RGS (Reflection Grating Spectrometer, den Herder et al. 2001) data, which provide high resolution soft X-ray spectra in the range of 5 to 35 Å. Our aim is to model the absorption edges in the soft X-rays to determine the hydrogen column density along the line of sight towards XTE J1752−223.

We extracted RGS spectra using the *rgsproc* within SAS v11.0.0 with the latest calibration files available as of Dec. 2011. We grouped the RGS spectra with *specgroup* tool so that each spectral channel will have at least 100 counts and the instrumental resolution will not be oversampled more than a factor of 3.

Given the X-ray flux of the source at the time of the observation we also checked the RGS observation against any affect of photon pile-up. For this purpose we used the fluxed RGS X-ray spectra, as given by the Browsing Interface for RGS data (BIRD), and checked the flux on each CCD against the limits given in the XMM-Newton User's Handbook[7]. This comparison showed us that even though there was a photon pile-up it was smaller than 2%. This is also thanks to the fact that the observation was performed with double-node readout for RGS1 and RGS2. Such a small amount of saturation would have only minimal, if any, affects on the depths of individual absorption edges.

2.5. *Optical & NIR observations*

[7] http://xmm.esac.esa.int/external/xmm_user_support/documentation/uhb/index.html

In addition to the X-ray observations, we analyzed the O/NIR SMARTS data (I and H band) obtained with the CTIO 1.3m telescope, during MJD 55,240–55,390 covering 150 days of the outburst decay. With the help of IRAF V2.14, we conducted photometry using the PSF (Point Spread Function) fitting due to the crowded region towards the source (see Russell et al. 2011, for the high resolution NIR image). Then we selected five comparison stars in the FOV as non-variables, and went through the standard routines to get the actual magnitudes (see Buxton et al. 2012 for standard procedures). The magnitudes we obtained could be affected by a nearby source, especially in the H band due to the poor observational conditions and the resolution of the telescope. The results are shown in Figs .1 and 2.

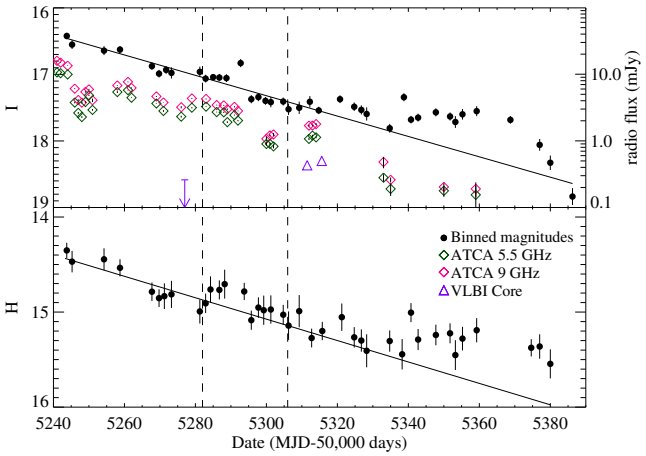

Figure 2. The evolution of O/NIR magnitudes, and radio fluxes during the decay. The O/NIR magnitudes are binned to reduce errors. The solid lines indicate an exponentially decaying emission possibly from the outer disk, which are shown to bring up the jet component. The radio data are added with colored diamonds and triangles (see legend). The errors on radio before MJD 55,320 are smaller than the symbol size. The dates of the fast transition and the ISGRI observation are indicated by solid lines on MJD 55,282 and 306, respectively.

2.6. *Radio*

The *Australia Telescope Compact Array* (*ATCA*) provided the evolution of the source throughout the decay in radio in two bands, 5.5 and 9 GHz. The peak fluxes in two bands were yielded with the help of the radio interferometry data reduction package, *Miriad* (Sault et al. 1995), and more details in radio for this source will follow in Brocksopp et al. (in prep). In addition, the *Very Long Baseline Interferometry* (*VLBI*) also conducted a few observations during the decay. The high resolution of *VLBI* made it possible to resolve a compact jet core on MJD 55,311 and 55,315 and the radio flux values reported by Yang et al. (2011) were used in this paper in order to determine the time of compact jet formation.

3. ANALYSIS AND RESULTS

All *R*XTE and *S*wift spectra were fitted with a phenomenological model of disk blackbody (diskbb) plus power law with absorption. A smeared edge model (smedge, Ebisawa et al. 1994) was also added to the

RXTE spectrum to improve the χ^2 similar to previous work by this group (Kalemci et al. 2004, 2005, 2006a). For photoelectric absorption, we used Tuebingen-Boulder ISM absorption (*TBabs*), with the abundance values of Wilms et al. (2000) and the cross sections of Verner et al. (1996). This choice is discussed in more detail in Section 3.4. In addition, due to the close position of the source to the galactic plane ($b = +02°.11$), the Galactic ridge contribution was important at low luminosity levels for *RXTE*. To take into account the Galactic ridge emission, an additional powerlaw was added to the spectral fit after MJD 55,310, fixing the index to 2.1 and normalization to 1.209 10^{-2} based on values given in Revnivtsev (2003). The rms amplitudes were corrected for ridge after MJD 55,303 as well as for background emission following Berger & van der Klis (1994).

3.1. *Multiwavelength evolution*

Fig.1 shows the evolution of the X-ray spectral and temporal propertes as well as the evoluton in O/NIR magnitudes. The vertical line on MJD 55,282 indicates the transition in timing due to the fast change in the rms. An increase in the power-law flux accompanies the increase in the rms amplitude of variability. The X-ray flux continued to increase for a couple of days after the transition, whilst the photon index remained the same until the peak in X-ray flux. As the X-ray flux started to decay, the photon index abruptly decreased to ∼1.7. The spectrum continued to harden and the index levelled off around 1.6. A secondary peak was also observed in X-rays after MJD 55,340.

The SMARTS optical and NIR observations showed interesting behavior as shown in Figs .1 and 2. Some ripples are present in the light curves, at around MJD 55,280 and MJD 55,320 followed by a large increase in flux starting around MJD 55,340 coinciding with the increase in the X-ray flux (Russell et al. 2011). The bump at MJD 55,280 in the H band coincides with the timing transition, and the bump at MJD 55,320 in the I band coincides with the end of hardening in the X-ray spectra.

Fig.2 also shows the evolution of radio flux during outburst decay at different wavelengths from different observations. The green and red diamonds are from *ATCA* at 5.5 GHz and 9 GHz, respectively. We also showed the H and I band magnitudes to associate changes in radio to the changes in optical/NIR. For clarity the H and I magnitudes are binned for every couple of days. Until MJD 55,320, the radio spectrum is optically thin. At MJD 55,311 and MJD 55,315, the radio core is detected with the *VLBI*, while the *ATCA* radio spectrum was still optically thin. This indicates that there is contamination in the radio data, and the *ATCA* flux includes emission from a compact jet and some other interaction. The detection of the core corresponds to a little flare that can be seen in the I band. Around MJD 55,335 the ATCA spectrum is consistent with a flat spetrum, and this is where the flux in I, H band, and X-rays increase.

3.2. *Timing evolution during the brightening*

As distinct multiwavelength changes occur during the brightening after MJD 55,340, we decided to check whether there are any changes in the PSD at the same time. The evolution of PSDs is shown in Fig. 3. We

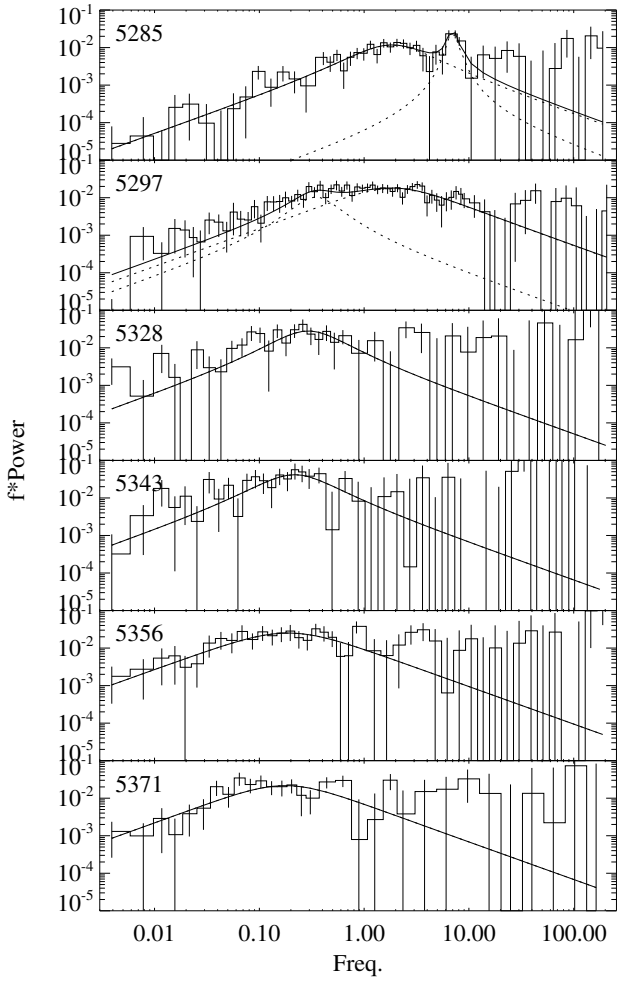

Figure 3. Several selected PSDs from the intermediate state to low flux hard state. The vertical axes are frequency*power and the dates (MJD-50,000) are indicated on the left of each panel. The peak of the Lorentzian gradually decreases, and no clear difference before, on, and after the NIR peak at the bottom three panels, respectively.

started from day MJD 55,285, during the first X-ray peak, and go down in flux to compare observations before and during the peak with similar fluxes. At MJD 55,285 two Lorentzians are required to fit the data, and the first Lorentzian peaks at ∼1.83 Hz. The rms amplitude of variability is ∼18.72%. At MJD 55,297 the spectrum is now hard (Γ∼1.7), and the rms amplitude is higher (∼25.46%). Still two Lorentzians are required to fit the data, but the peak frequency of the first Lorentzian is shifted down to ∼0.35 Hz. For the rest shown in Fig. 3, a single Lorentzian is enough to fit the data. At MJD 55,328 and MJD 55,356 the X-ray fluxes are almost the same with similar spectral parameters. The PSDs are also similar, and the rms and peak frequencies are consistent within errors. Likewise, the PSDs at MJD 55,343 and MJD 55,371 are also at similar flux levels, and show no significant change in spectral and timing properties (see Table 1 for parameters). Even though the statistics are not good enough to demonstrate a significant difference (or there lack off), the timing properties appear not to change before and during the flare, and similar X-ray

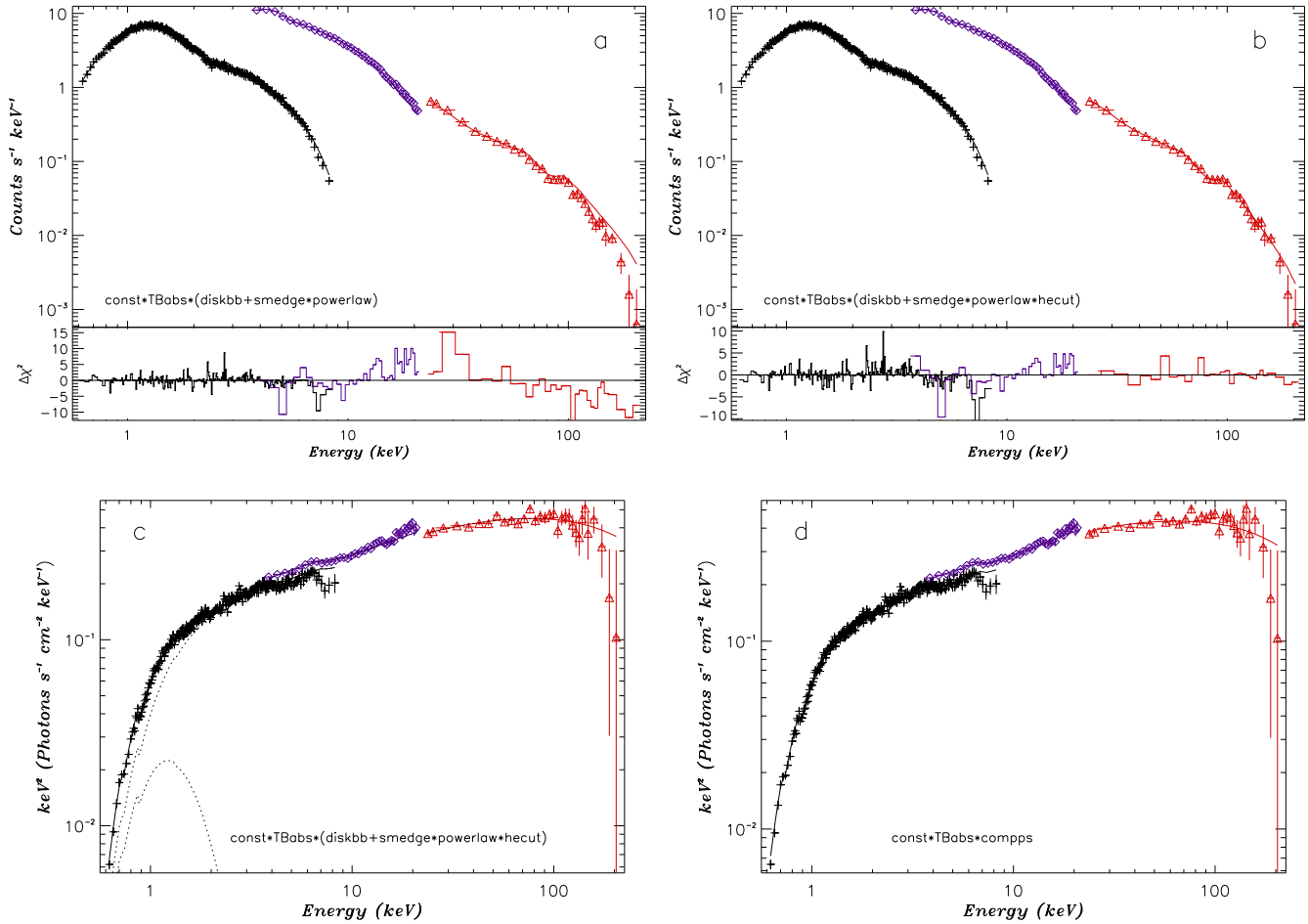

Figure 4. Spectral fits to the *Swift* XRT (shown with + sign, colored black in the online version), *RXTE* PCA (shown with diamonds, colored purple in the online version) and *INTEGRAL* ISGRI data (shown with triangles, colored red in the online version). a) Count spectrum and fit with a power-law and disk blackbody. b) Count spectrum and fit with a power-law and a high energy cut-off and disk blackbody. c) Unfolded spectrum with high energy cut-off. d) Unfolded spectrum with Comptonization model compps.

Table 2
The best fit parameters for simultaneous XRT, PCA, and ISGRI spectra

Models	N_H	kT_{bb}, T_{in}[a]	τ[b]	$\Omega/2\pi$[c]	$kT_e(keV)$[d]	Γ	$E_{cut}(keV)$[e]	$E_{fold}(keV)$[f]	$\chi^2/(dof)$
CompPS+diskline	$0.60^{+0.02}_{-0.02}$	$0.28^{+0.01}_{-0.01}$	$1.24^{+0.24}_{-0.19}$	$0.53^{+0.11}_{-0.09}$	$105.2^{+14.8}_{-14.8}$	...	...	...	312(323)
power*highecut	$0.67^{+0.04}_{-0.04}$	$0.27^{+0.03}_{-0.02}$	...	...	...	$1.67^{+0.02}_{-0.02}$	$25.4^{+7.3}_{-7.6}$	$236.5^{+41.8}_{-32.2}$	342(323)

[a] The inner radius temperature of soft photons in multicolour disk.
[b] The vertical optical depth of the corona.
[c] The reflection factor.
[d] The electron temperature in the corona.
[e] The cut off energy.
[f] The folding energy.

spectral properties provide similar PSDs.

3.3. *Broadband X-ray spectrum*

To test whether spectral breaks disappear with the formation of jets, we conducted observations with the *INTEGRAL* Observatory. The ISGRI spectrum is combined with contemporaneous *RXTE* PCA data. We started with our standard model that consists of absorption, diskbb, smedge and power-law. We saw strong residuals indicating a high energy cut-off component in the fit (see Fig. 4.a). Adding a high energy cut-off (*highecut*) significantly improved the fit (F-test results in a chance probability of 10^{-20}, see Fig. 4.b and c.). The fit parameters can be found in Table 2.

Moreover, we also tried physical models and tried to establish whether an iron line is present in the spectrum. We fit the combined ISGRI, PCA, XRT spectrum first with the thermal Comptonization code, *CompPS* (Poutanen & Svensson 1996, see Fig. 4.d) and obtained a reasonable fit. The statistics in the XRT data were not good at the iron line region. We added *diskline* (Fabian et al. 1989) to model the iron line emission at around

Table 3
Resulting Hydrogen column density values obtained from fits to individual absorption edges in the RGS data. Values are in units of 10^{22} cm^{-2}

	O	Fe	Ne	Mg	Average[a]
ISM[b]	1.04±0.05	0.88±0.04	1.17±0.12	1.08±0.18	0.96±0.03
Solar[c]	1.04±0.05	0.73±0.04	1.17±0.12	0.99±0.14	0.88±0.03

[a] Error weighted averages of the values found from individual edges.
[b] As given by Wilms et al. (2000).
[c] As presented by Asplund et al. (2009).

∼6.4 keV. The improvement in the fit was not significant. Our dataset do not allow us to constrain the iron line parameters of this source at the time of the *INTEGRAL* observation.

3.4. *Distance to the source*

In order to measure the interstellar X-ray absorption in a way that is independent from assumptions on the intrinsic X-ray spectral properties of the source, we model individual absorption edges of the elements O, Ne, Fe, and Mg. For this purpose we only use the X-ray grating observation of the source obtained with the RGS on board *XMM*.

To measure the Hydrogen column density towards XTE J1752−223, we followed a method similar to Durant & van Kerkwijk (2006) and Güver et al. (2010). We selected only a small wavelength range for each edge; 8.5−10.5Å region for Mg, 13.5−15.0Å for Ne, 16.0−18.0Å for Fe, and 20.0-25.0Å for the O edge (note that in this wavelength range RGS2 has no sensitivity because of a CCD failure early in the mission, hence we did not include data from RGS2 for the O edge). We assumed that the continuum in these small intervals can be modelled with a powerlaw function and modelled each edge using the *tbnew*[8] model (Wilms et al. 2011, in prep). For spectral modelling we used XSPEC 12.7.0 (Arnaud 1996). We used the elemental photoelectric absorption cross-sections as given by Verner et al. (1996). Finally we performed the fits both assuming ISM and solar abundances as given by Wilms et al. (2000) and Asplund et al. (2009), respectively. We present the resulting Hydrogen column density values in Table 3 for each element and show our fits to the data in Fig 5.

Following the method outlined in Güver et al. (2010) and the relations presented by Güver & Özel (2009) and Cardelli et al. (1989), the Hydrogen column density we measure assuming an ISM abundance results in an optical extinction of A_V=4.34±0.22 mag or near-infrared extinction of A_{K_s}= 0.49±0.09 mag. Similarly assuming a solar abundance we get an optical extinction of A_V=3.98±0.21 or near-infrared extinction of A_{K_s}=0.46±0.08 mag.

3.5. *Near-IR extinction in the direction of the XTE J1752−223*

Near-IR observations of red clump stars have been used to map the extinction as a function of distance along a given line of sight in the Galaxy, as reported in a number of studies by Paczynski & Stanek (1998); López-Corredoira et al. (2002); Cabrera-Lavers et al. (2005); Nishiyama et al. (2006). As they have a very narrow luminosity function (especially in the near-infrared) and they can be easily isolated from a colour magnitude diagram, they have been largely used as standard candles in describing the geometry in the inner Galaxy (Cabrera-Lavers et al. 2007, 2008). For all the above, this population becomes a very powerful tool both for tracing and modeling the interstellar extinction in the more obscured areas of the Milky Way (see, e.g. Drimmel et al. (2003), or Marshall et al. (2006)).

These stars have also been used to estimate the distances of X-ray sources by comparing the estimates for the running of extinction with the distance derived from the NIR data with the intrinsic extinction of the source derived from their X-ray data, with very successful results (see, e.g., Durant & van Kerkwijk (2006); Castro-Tirado et al. (2008); Güver et al. (2010)). Here, we follow a similar method to map the evolution of extinction with distance in the direction of XTE J1752-223 by using photometric data from the 2MASS survey (Skrutskie et al. 2006).

In Fig. 6 (right) we show the derived evolution of the extinction as we move to the inner Galaxy in the direction of XTE J1752-223 (l=6°.42 , b=+2°.11), while the region formed by the red clump stars can be seen in the colour-magnitude diagram (see Fig. 6, left). As it can be seen, the extinction increases up to 4.5–5 kpc due to the interstellar dust in the Galactic plane in this direction, and remains nearly constant for distances larger than these. We observe this flattening since we have reached the bulge component at this distance along the line of sight, making harder to trace accurately the extinction for larger distances. The red clump sources for the Bulge at a galactic latitude of 2 deg above the plane completely dominates the star counts at this distance, and the (few) red clump sources for the Galactic disc are completely diluted. Hence the derived extinction for distances bigger than 5 kpc is completely biased to the values for the Galactic Bulge and nothing can be said for the extinction at greater distances. Therefore, this method of using red clump stars unfortunately has limited capability in terms of measuring the distance to XTE J1752-223. However it is reasonably clear that, based on the extinction values we obtained for the source from X-ray spectroscopy and assuming that at least a significant part of the X-ray absorption is not due to intrinsic absorption, XTE J1752-223 cannot be closer than at least 5 kpc

4. DISCUSSION

4.1. *State transitions and jets*

The results of X-ray monitoring and the O/NIR lightcurves are shown in Fig. 1, and the radio evolution is included in Fig. 2. Judging by the whole evolution of the

[8] http://pulsar.sternwarte.uni-erlangen.de/wilms/research/tbabs/

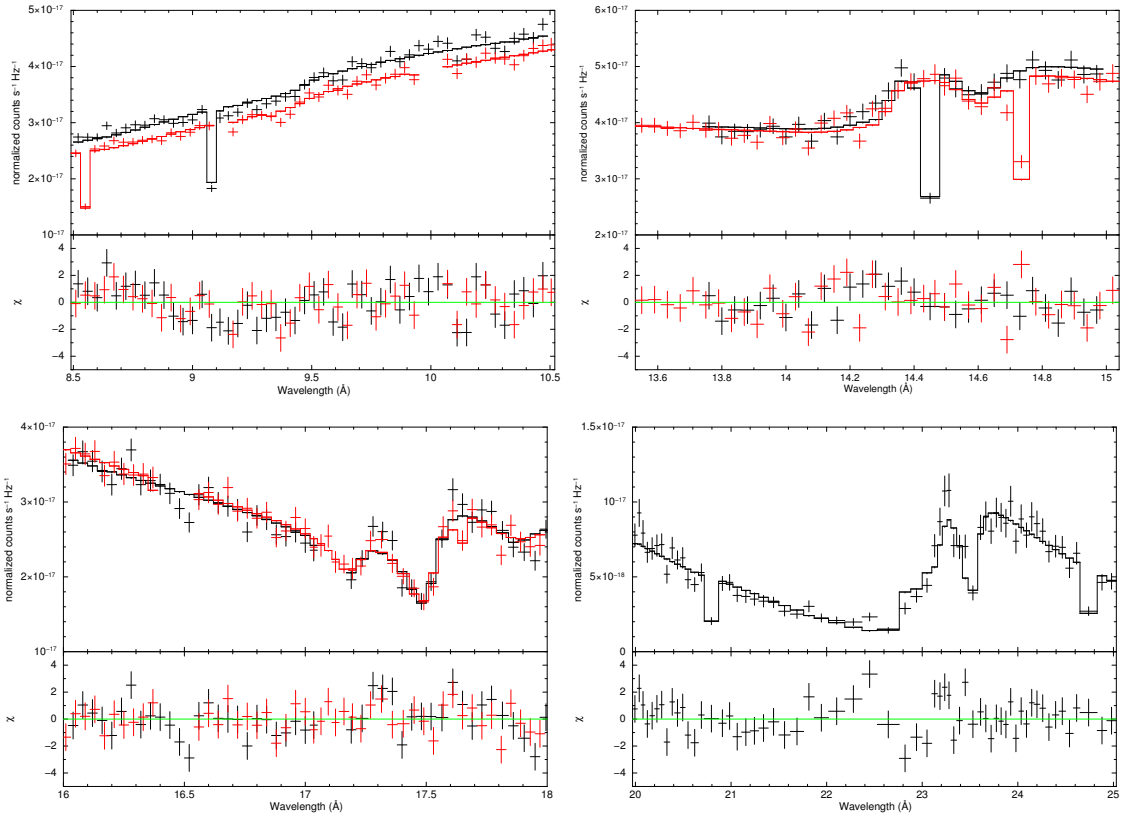

Figure 5. RGS1 (black) and RGS2 (red) data at the Mg (upper left), Ne (upper right), Fe (lower left), and O (lower right panel) absorption edge regions are shown in the upper panels of each plot. Lower panels show the residuals from the best fit model. Sharp features are due to CCD gaps in the RGS detector.

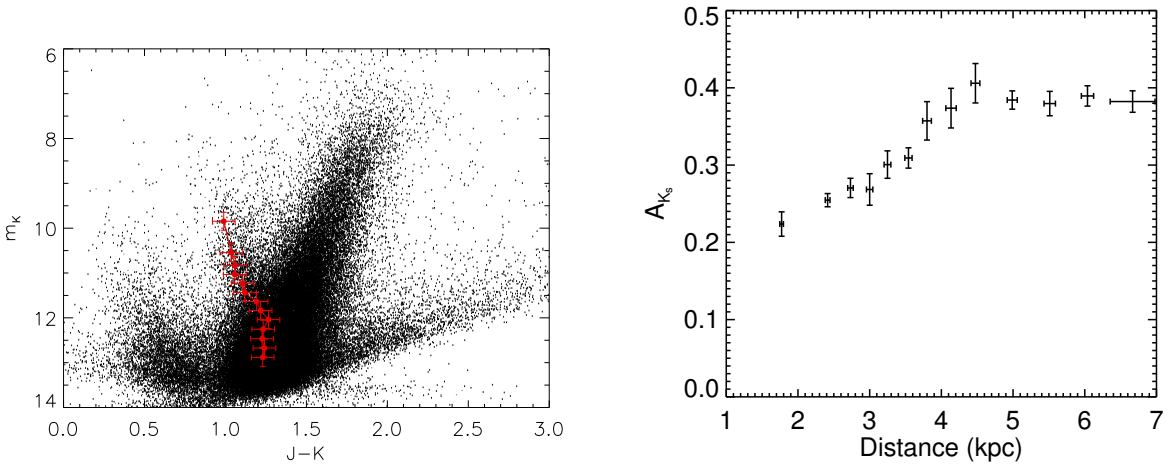

Figure 6. Left: Near-IR colour-magnitude diagram for the field centered around XTE J1752- 223. Red crosses show points of maximum density of red clump stars for each individual magnitude bin and their uncertainties. Right: Evolution of near-IR extinction in the direction of XTE J1752-223 as derived from the 2MASS archive.

ATCA radio observation and *VLBI* detections, the first small flare in NIR on MJD 55,282 (which is more prominent in the H band) is probably not from the jet as the jets seem to start forming after about MJD 55,300. Another small flare in the I band starting on MJD 55,305 however, seems coincident with both the *VLBI* detection of the core on MJD 55,312 and a small excess of the *ATCA* observations. *ATCA* spectrum hardens and become flat on MJD 55,350. This spectral evolution coincides with the larger flare seen in both the I and the H band starting at MJD 55,340. A compact jet is probably dominating the O/NIR and radio emission after MJD 55340. Such a relation between the radio spectral properties and the O/NIR rise is also seen for GX 339-4 (Corbel et al. 2012; Dinçer et al. 2012; Kalemci et al. 2012).

If the emission from a compact jet dominates the X-ray emission during the second long flare between MJD 55,340 and 55,380 (Russell et al. 2012) one could expect some change in the timing properties before and after the peak. We did not observe a significant change in the PSDs, their rms amplitudes, and the peak frequencies when the compact jet is present. However, because the errors of the peak frequencies in these datasets are not negligible, ∼30%, timing studies for brighter sources might be more useful to discuss the effects of jets on timing.

4.2. *Spectral breaks in hard X-rays*

The presence of spectral breaks is well established during the transition to (or from) the hard state (Kalemci et al. 2005; Motta et al. 2009). There is some indication that the breaks disappear after the jet turns on based on spectral fitting of data from HEXTE on *RXTE* Kalemci et al. (2006b). However, there is no conclusive evidence that relates the jet formation to the evolution of spetral breaks as the short monitoring observations with *RXTE* often lack the statistics required to characterize this evolution. To obtain better statistics in hard X-rays we triggered our *INTEGRAL* observation around the time that the spectral index is hardest. The observation took place just before the core is detected wth the $VLBI$. The broadband combined spectrum clearly shows a break, with a folding energy at ~ 237 keV. This result is consistent with earlier work, a cut-off is present before a strong compact jet is launched. Unfortunately the timing of the observation did not allow us to test the hypothesis that the cut-offs disappear after the jets turned on. The hard X-ray spectrum of the source is consistent with thermal Comptonization.

4.3. *Distance*

The method using red clump stars provides a lower limit to the distance to the source of > 5 kpc. Shaposhnikov et al. (2010) estimate the distance of the source as about 3.5 kpc. At this distance the galactic extinction is about 60% of what we infer from the absorption edges observed with *XMM* RGS. Assuming that the intrinsic absorption in this source is not as high as 2 magnitudes in the optical, this distance estimate is incompatible with our results. Such a high intrinsic absorption seems hard to understand given that no dips in the X-rays have been observed, which could have been interpreted as neutral matter absorbing X-rays emitted from the boundary layer. It has been found by Miller et al. (2009) that the X-ray absorption as derived from photoelectric absorption edges remains constant as the luminosity and spectral states of X-ray binaries including black hole systems vary. This finding suggests that the ISM strongly dominates the measured neutral Hydrogen column density in the spectra of X-ray binaries.

Also, possible uncertainties in the extinction law used for deriving the interstellar extinction (see e.g. Nishiyama et al. 2009; Gonzalez-Fernandez 2012, in press) cannot support such high differences with respect to the estimate by Shaposhnikov et al. (2010), as the differences are well accounted within the error bars shown in Fig. 6. Hence the assumption of XTE J1752-223 being no closer than 5 kpc is not produced by uncertainties in the NIR extinction measurements.

We note that the distance of 3.5 kpc is also not compatible with the overall behavior of GBHTs in terms of their transition luminosities (Maccarone 2003; Ratti et al. 2012). As shown in Kalemci et al. (2012), the overall luminosity evolution of this source become compatible with other black hole transients if we assume a distance around 8 kpc, and a distance of 3.5 kpc would make this source behaving quite differently with respect to the other black hole binary systems. Future observations of this source at a new outburst can test our measurements and provide clues about the any variabilities in the amount of X-ray absorption, which would be a direct evidence of intrinsic absorption.

5. SUMMARY AND CONCLUSIONS

In this work we analyzed data from the Galactic black hole binary XTE J1752−223 from the radio band all the way to hard X-rays during its outburst decay in 2010. We investigated the evolution of X-ray spectral and temporal properties of the source using *RXTE* and *SWIFT*, and compared the results to the evolution of fluxes in the I and H band *SMARTS* data, and also to the spectral evolution of the *ATCA* radio data. We also studied the $XMM-Newton$ RGS data to find the extinction towards the source. The important results from this analysis are summarized below:

- We showed that the detection of the radio core with the $VLBI$ corresponds to a small flare in the I band flux. Subsequently, both the I and H band flux increase showing a secondary outburst.
- The secondary outburst coincides with the *ATCA* radio data becoming optically thick, relating the compact jet to the O/NIR changes.
- The short term X-ray timing properties do not show a significant change during changes in the O/NIR and radio properties.
- The broadband X-ray spectrum including *INTEGRAL* ISGRI indicates a high energy cut-off, which is also seen in other sources before strong compact jets are observed. The spectrum is consistent with thermal Comptonization.
- We showed that the distance to the source cannot be less than 5kpc.

YYC, EK, TD and SC acknowledge support from FP7 Initial Training Network Black Hole Universe, ITN 215212. EK and TD acknowledges TÜBİTAK grant 111T222. JAT acknowledges partial support from NASA *Swift* Guest Observer grant NNX10AK36G and also from the NASA Astrophysics Data Analysis Program grant NNX11AF84G. EK thanks Sinan Alis for his helps in IRAF analysis. Authors thank all scientists who contributed to the Tübingen Timing Tools.

REFERENCES

????
08. 1
Arnaud, K. A. 1996, in ASP Conf. Ser. 101: Astronomical Data Analysis Software and Systems V, Vol. 5, 17
Asplund, M., Grevesse, N., Sauval, A. J., & Scott, P. 2009, ARA&A, 47, 481
Belloni, T., Psaltis, D., & van der Klis, M. 2002, ApJ, 572, 392
Belloni, T. M. 2010, in Lecture Notes in Physics, Berlin Springer Verlag, Vol. 794, Lecture Notes in Physics, Berlin Springer Verlag, ed. T. Belloni, 53–+
Berger, M., & van der Klis, M. 1994, A&A, 292, 175
Buxton, M. M., Bailyn, C. D., Capelo, H. L., Chatterjee, R., Dinçer, T., Kalemci, E., & Tomsick, J. A. 2012, AJ, 143, 130
Caballero García, M. D., et al. 2007, ApJ, 669, 534
Cabrera-Lavers, A., Garzón, F., & Hammersley, P. L. 2005, A&A, 433, 173
Cabrera-Lavers, A., González-Fernández, C., Garzón, F., Hammersley, P. L., & López-Corredoira, M. 2008, A&A, 491, 781
Cabrera-Lavers, A., Hammersley, P. L., González-Fernández, C., López-Corredoira, M., Garzón, F., & Mahoney, T. J. 2007, A&A, 465, 825
Cadolle Bel, M., et al. 2004, A&A, 426, 659
Cardelli, J. A., Clayton, G. C., & Mathis, J. S. 1989, ApJ, 345, 245
Castro-Tirado, A. J., et al. 2008, Nature, 455, 506
Corbel, S., Coriat, M., Brocksopp, C., Tzioumis, A. K., Fender, R. P., Tomsick, J. A., Buxton, M. M., & Bailyn, C. D. 2012, MNRAS, accepted, 2012arXiv1211.1600C
Corbel, S., Fender, R. P., Tzioumis, A. K., Nowak, M., McIntyre, V., Durouchoux, P., & Sood, R. 2000, A&A, 359, 251
Corbel, S., Nowak, M. A., Fender, R. P., Tzioumis, A. K., & Markoff, S. 2003, A&A, 400, 1007
Coriat, M., Corbel, S., Buxton, M. M., Bailyn, C. D., Tomsick, J. A., Körding, E., & Kalemci, E. 2009, MNRAS, 400, 123
Curran, P. A., Maccarone, T. J., Casella, P., Evans, P. A., Landsman, W., Krimm, H. A., Brocksopp, C., & Still, M. 2011, MNRAS, 410, 541
den Herder, J. W., et al. 2001, A&A, 365, L7
Dinçer, T., Kalemci, E., Buxton, M. M., Bailyn, C. D., Tomsick, J. A., & Corbel, S. 2012, ApJ, 753, 55
Drimmel, R., Cabrera-Lavers, A., & López-Corredoira, M. 2003, A&A, 409, 205
Durant, M., & van Kerkwijk, M. H. 2006, ApJ, 650, 1070
Ebisawa, K., et al. 1994, PASJ, 46, 375
Fabian, A. C., Rees, M. J., Stella, L., & White, N. E. 1989, MNRAS, 238, 729
Falcke, H., Körding, E., & Markoff, S. 2004, A&A, 414, 895
Fender, R. P. 2001, MNRAS, 322, 31
Gonzalez-Fernandez, C. 2012, in press
Güver, T., & Özel, F. 2009, mnras, 400, 2050
Güver, T., Özel, F., Cabrera-Lavers, A., & Wroblewski, P. 2010, apj, 712, 964
Joinet, A., Kalemci, E., & Senziani, F. 2008, ApJ, 679, 655
Kalemci, E., Dincer, T., Tomsick, J. A., Buxton, M., Bailyn, C., & Chun, Y. Y. 2012, ApJ, submitted
Kalemci, E., Tomsick, J. A., Buxton, M. M., Rothschild, R. E., Pottschmidt, K., Corbel, S., Brocksopp, C., & Kaaret, P. 2005, ApJ, 622, 508
Kalemci, E., Tomsick, J. A., Rothschild, R. E., Pottschmidt, K., Corbel, S., & Kaaret, P. 2006a, ApJ, 639, 340
Kalemci, E., Tomsick, J. A., Rothschild, R. E., Pottschmidt, K., & Kaaret, P. 2004, ApJ, 603, 231
Kalemci, E., Tomsick, J. A., Rothschild, R. E., Pottschmidt, K., Migliari, S., Corbel, S., & Kaaret, P. 2006b, in VI Microquasar Workshop: Microquasars and Beyond
Körding, E., Falcke, H., & Corbel, S. 2006, A&A, 456, 439
Körding, E. G., Migliari, S., Fender, R., Belloni, T., Knigge, C., & McHardy, I. 2007, MNRAS, 380, 301
López-Corredoira, M., Cabrera-Lavers, A., Garzón, F., & Hammersley, P. L. 2002, A&A, 394, 883
Maccarone, T. J. 2003, A&A, 409, 697
Markwardt, C. B., Barthelmy, S. D., Evans, P. A., & Swank, J. H. 2009a, The Astronomer's Telegram, 2261, 1
Markwardt, C. B., et al. 2009b, The Astronomer's Telegram, 2258, 1
Marshall, D. J., Robin, A. C., Reylé, C., Schultheis, M., & Picaud, S. 2006, A&A, 453, 635
McClintock, J. E., & Remillard, R. A. 2006, Black hole binaries, ed. Lewin, W. H. G. & van der Klis, M., 157–213
Merloni, A., Heinz, S., & di Matteo, T. 2003, MNRAS, 345, 1057
Miller, J. M., Cackett, E. M., & Reis, R. C. 2009, ApJ, 707, L77
Miller-Jones, J. C. A., Jonker, P. G., Ratti, E. M., Torres, M. A. P., Brocksopp, C., Yang, J., & Morrell, N. I. 2011, ArXiv e-prints
Miyakawa, T., Yamaoka, K., Homan, J., Saito, K., Dotani, T., Yoshida, A., & Inoue, H. 2008, PASJ, 60, 637
Miyamoto, S., & Kitamoto, S. 1989, Nature, 342, 773
Motta, S., Belloni, T., & Homan, J. 2009, MNRAS, 400, 1603
Muñoz-Darias, T., Motta, S., Pawar, D., Belloni, T. M., Campana, S., & Bhattacharya, D. 2010, MNRAS, 404, L94
Nakahira, S., et al. 2010, PASJ, 62, L27+
Nishiyama, S., Tamura, M., Hatano, H., Kato, D., Tanabé, T., Sugitani, K., & Nagata, T. 2009, ApJ, 696, 1407
Nishiyama, S., et al. 2006, ApJ, 647, 1093
Paczynski, B., & Stanek, K. Z. 1998, ApJ, 494, L219
Pottschmidt, K. 2002, PhD Thesis, Univ. of Tübingen
Poutanen, J., & Svensson, R. 1996, ApJ, 470, 249
Ratti, E. M., et al. 2012, MNRAS, 3053
Reis, R. C., et al. 2011, MNRAS, 410, 2497
Revnivtsev, M. 2003, A&A, 410, 865
Russell, D. M., Maitra, D., Dunn, R. J. H., & Markoff, S. 2010, MNRAS, 405, 1759
Russell, D. M., Miller-Jones, J. C. A., Maccarone, T. J., Yang, Y. J., Fender, R. P., & Lewis, F. 2011, ApJ, 739, L19
Russell, D. M., et al. 2012, MNRAS, 419, 1740
Sault, R. J., Teuben, P. J., & Wright, M. C. H. 1995, in Astronomical Society of the Pacific Conference Series, Vol. 77, Astronomical Data Analysis Software and Systems IV, ed. R. A. Shaw, H. E. Payne, & J. J. E. Hayes, 433
Shaposhnikov, N. 2010, The Astronomer's Telegram, 2391, 1
Shaposhnikov, N., Markwardt, C., Swank, J., & Krimm, H. 2010, ApJ, 723, 1817
Skrutskie, M. F., et al. 2006, AJ, 131, 1163
Verner, D. A., Ferland, G. J., Korista, K. T., & Yakovlev, D. G. 1996, ApJ, 465, 487
Wilms, J., Allen, A., & McCray, R. 2000, ApJ, 542, 914
Wilms, J., Juett, A., Schulz, N., & Nowak, M. 2011, in prep
Yang, J., Paragi, Z., Corbel, S., Gurvits, L. I., Campbell, R. M., & Brocksopp, C. 2011, MNRAS, 418, L25
Zhang, W., Jahoda, K., Swank, J. H., Morgan, E. H., & Giles, A. B. 1995, ApJ, 449, 930